Precision control of single-molecule electrical junctions

WOLFGANG HAISS[1]*, CHANGSHENG WANG[2], IAIN GRACE[3], ANDREI S. BATSANOV[2], DAVID J. SCHIFFRIN[1], SIMON J. HIGGINS[1], MARTIN R. BRYCE[2], COLIN J. LAMBERT[3] AND RICHARD J. NICHOLS[1]

[1]Centre for Nanoscale Science and Department of Chemistry, University of Liverpool, L69 7ZD, UK
[2]Department of Chemistry and Centre for Molecular and Nanoscale Electronics, University of Durham, Durham DH1 3LE, UK
[3]Department of Physics, Lancaster University, Lancaster LA1 4YB, UK
*e-mail: w.h.haiss@liv.ac.uk

Published online: 26 November 2006; doi:10.1038/nmat1781

There is much discussion of molecules as components for future electronic devices. However, the contacts, the local environment and the temperature can all affect their electrical properties. This sensitivity, particularly at the single-molecule level, may limit the use of molecules as active electrical components, and therefore it is important to design and evaluate molecular junctions with a robust and stable electrical response over a wide range of junction configurations and temperatures. Here we report an approach to monitor the electrical properties of single-molecule junctions, which involves precise control of the contact spacing and tilt angle of the molecule. Comparison with *ab initio* transport calculations shows that the tilt-angle dependence of the electrical conductance is a sensitive spectroscopic probe, providing information about the position of the Fermi energy. It is also shown that the electrical properties of flexible molecules are dependent on temperature, whereas those of molecules designed for their rigidity are not.

In recent years it has been possible to position single molecules in electrical junctions[1–6], opening up a lively debate about their possible future use in nanoelectronic circuits. Molecular and nanoscale structures have been shown to be capable of basic electronic functions such as rectification, negative differential resistance and single-electron transistor behaviour[7–12]. These observations show that molecular-electronic functions can be controlled through chemical manipulation. However, speculation about the imminent application of molecules in nanoelectronic circuits may be premature, as there are still important issues to be resolved, including the reliable wiring of molecules, device interconnectivity in nanocircuits and thermal stability of molecular devices.

The difficulty in engineering electrode contact separations to subnanometre precision means that, for practical devices, molecules bridging the contacts should show reliable electrical performance over a range of contact spacing and temperature. Here, it is demonstrated that contact geometry and thermal fluctuations can be systematically controlled, through precise control of the nanoelectrode gap spacing, allowing molecules to be tilted or stretched, and by engineering the intrinsic rigidity of the molecules.

We first compare the electrical behaviour of the long-axially rigid molecular wires (namely 1,4-bis[4-(acetylsulphanyl)phenylethynyl]-2,6-dimethoxybenzene (molecule A, shown in Fig. 1e) with that of the flexible molecule 1,9-nonanedithiol (molecule B). The $I(t)$ and $I(s)$ methods previously developed by Haiss *et al.*, using scanning tunnelling microscopy (STM), were used for the measurement of single-molecule conductance[2,3,13,14]. The starting point for these measurements is the adsorption of a low coverage of an α,ω-dithiol molecule on a Au(111) surface. This condition results in flat-lying molecules and enables the formation of single-molecule wires with high probability. To attach a molecule to the STM tip (Au), the tip is lowered onto the surface by fixing the tunnelling current I_0 at relatively high values and then lifted, whilst keeping a constant position in the x–y plane. The current decay shows

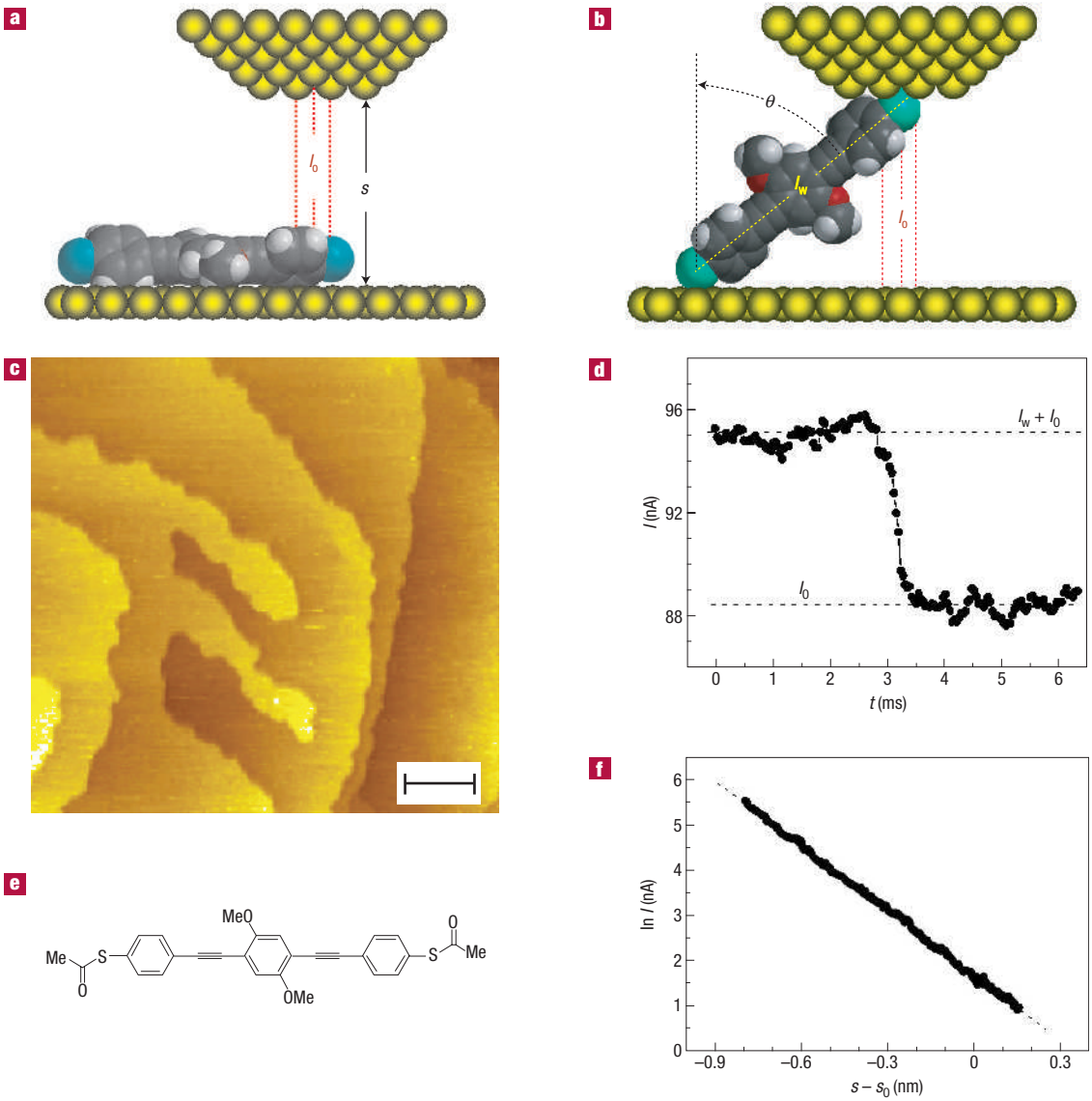

Figure 1 Representation of the experimental procedures used to measure the electrical conductance of a single molecule at a well-defined contact separation. **a**, Schematic representation of molecule A before formation of a contact to the STM tip. The tip–sample separation s is determined by the set-point current I_0. **b**, After formation of a contact to the STM tip, molecule A may show a maximum tilt angle (θ). **c**, STM image of the Au(111) sample surface after adsorption of A, showing extended atomically flat terraces separated by monoatomic steps; scale bar, 50 nm. **d**, Typical current jump attributed to the breaking of a molecular wire between tip and sample. **e**, Structure of A. **f**, Typical $\ln I(s)$ scan used for the calibration of $s(I)$.

distinctive current plateaux (of height I_w) when molecular wires bridge the gap between the tip and substrate, whereas in the absence of wire formation the current simply decreases nearly exponentially with tip–sample separation. As discussed previously, the current plateaux have been related to electron tunnelling through molecular wires bridging the STM tip and the substrate[2,3]. Statistical analysis of the data using histogram plots has shown that the current-plateau values group themselves into discrete values, which are integer multiples of a lowest value. The lowest current peak in the histogram (I_M) corresponds to a single molecule with conductance G_1, whereas the next discrete conductance step (G_2) has been assigned to conduction through two wires and so on. This is referred to as the '$I(s)$ method'[3] (see the Supplementary Information).

An alternative method has been recently published, which is referred to as the '$I(t)$ method'[2]. This involves holding the Au STM tip at a given distance above the substrate whilst monitoring current jumps as molecular wires bridging the tip and substrate form and subsequently break. It has been previously shown that both the $I(s)$ and the $I(t)$ method result in the same single-molecule conductance (G_1) for alkanedithiols[2]. The experimental results of the present study have been obtained with the $I(t)$ technique, as it offers the unique possibility of controlling s to better than 0.05 nm and hence allows us to study the dependence of the single-molecule conductance on contact spacing. A schematic representation of molecule A before and after the formation of a molecular bridge is shown in Fig. 1a,b. For these measurements we prepared the tip and the sample by a flame-annealing process, which results

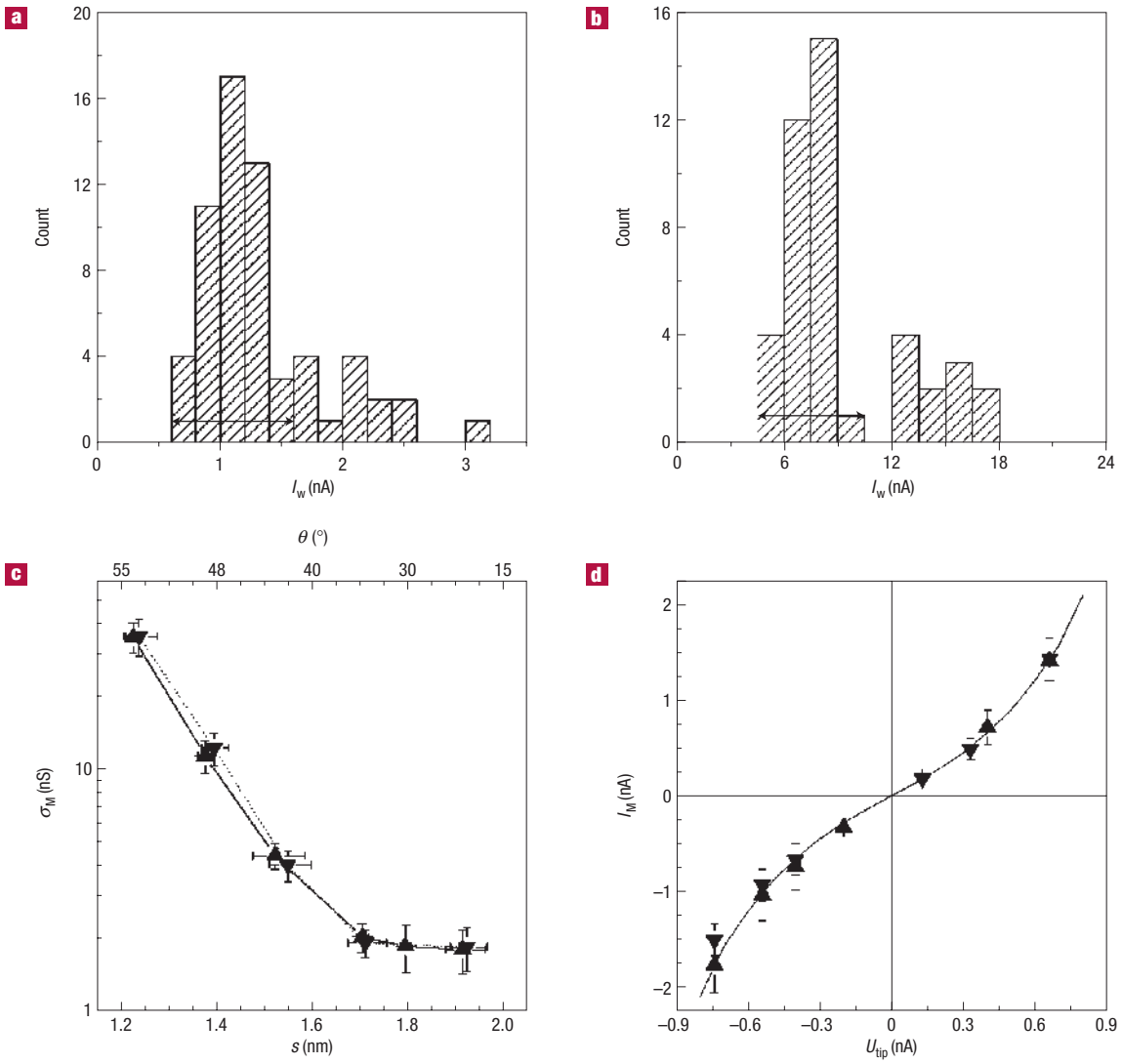

Figure 2 Experimental results obtained for the conductance of molecule A on Au(111). a, Histogram of current jumps observed at a set-point current of 4.4 ± 0.9 nA. **b**, Histogram of current jumps observed at a set-point current of 75 ± 13 nA. $U_{tip} = +0.6$ V and $T = 22$ °C in **a** and **b**. The double-headed arrows in **a** and **b** mark group 1 events, that is, current jumps, which are attributed to the attachment or detachment of single molecules. **c**, Single-molecule conductance of A measured at 77 °C (up triangles) and 22 °C (down triangles) in dependence on the tip–sample separation s. The tilt angle θ is shown on the top axis. **d**, Dependence of I_M on the applied bias measured at small tilt angles. The solid line shows a fit of the experimental data with the results of an *ab initio* calculation for a Fermi-level position of +0.2 V where both sulphur atoms are adsorbed in three-fold hollow sites. We divided the theoretical values by a constant factor of 2.3 to fit the experimental data and to facilitate a comparison of the calculated voltage dependence with the experimentally observed voltage dependence. Error bars in **c** and **d** represent the standard deviation of group 1 events.

in atomically flat (111) terraces extending up to several hundred nanometres separated by monoatomic steps (see Fig. 1c).

A typical current trace recorded by the $I(t)$ method during the breaking of a molecular bridge between the gold STM tip and gold substrate is shown in Fig. 1d. During this experiment, we disable the feedback loop of the STM so that current jumps resulting from molecular bridging can be recorded. I_0 is the set-point current, whereas I_w corresponds to the current flow through the molecular wire. It should be noted that I_0 controls s, with high I_0 corresponding to small s. For I_0 values of the order of 75 nA the tip–sample separation will be much smaller than the length of the bridging molecule and hence the molecule may show a considerable tilt. Figure 2a,b shows typical histograms of current jumps using values of I_0 of 4.4 and 75 nA respectively. The single-molecule current is calculated from group 1 events marked with the arrows.

We determined the current flowing through a single molecule (I_M) from histograms like the one shown in Fig. 2a, which we collected at different set-point currents and at different temperatures. We then calculated the corresponding single-molecule conductance (σ_M) simply by dividing I_M by the applied voltage. Below a critical set-point current (I_c) molecular wires can no longer span the gap. Using this value, and a current–distance calibration obtained from $I(s)$ scans taken during each experiment (see Fig. 1f as an example and the Methods section for details), the single-molecule conductance (σ_m) can be plotted versus the contact separation. For large s values, corresponding to the length of the fully extended molecule, an assignment of the tilt angle to the tip–sample separation is straightforward as areas having larger gaps cannot be bridged. For small tip–sample separations, in principle both fully tilted molecules having a tilt

angle θ (see Fig. 1b) and untilted molecules could bridge different parts of the gap at different sample locations. As the formation of molecular bridges is induced by the electric field between tip and sample, the most probable place for wire formation will be the area of the highest field strength, that is at the tip apex. This interpretation is corroborated by a comparison of current jump histograms collected at different tip–sample separations (see Fig. 2a,b and the Supplementary Information for details). If at small gap separations a larger distribution of tilt angles, ranging from 0 to θ degrees, were present, then this would be reflected in a significant broadening of the current-histogram data. Such a broadening of the histogram as the gap is made smaller is not observed, indicating that predominantly the fully tilted configuration is favoured. The uncertainty in the atomic configuration of the apex within the framework of the measurements is thus expected to lead to an acceptable uncertainty in the tilt angle as observed in the experiments.

The contact separation and tilt angle are defined in Fig. 1a,b respectively, whereas the dependence of σ_m on s for A is shown in Fig. 2c for 22 °C (down triangles) and 77 °C (up triangles). Within experimental uncertainly, conductance values are the same at these two temperatures over the whole range of s. The tilt angle (θ) is shown on the top axis. Figure 2d shows the voltage dependence of the current (I_M) flowing through a single molecule for two different temperatures. As expected for a symmetric adsorption geometry, $I_M(V)$ is symmetric with respect to the polarity. Interestingly, for these rigid molecules, no dependence of σ_M on temperature is observed over the entire range of θ and over the examined voltage range.

For comparison with Fig. 2c, the single-molecule conductance of the flexible molecule B as a function of s is shown in Fig. 3, determined using the same method as for A. In the case of molecule B, the contact separation is calculated, assuming an all-*trans* conformation standing perpendicular on the surface at the critical current (I_c). The two plots shown in Fig. 3 were taken at 28 °C (down triangles) and 75 °C (up triangles), showing a pronounced temperature dependence of σ_M for intermediate tip–sample separations (0.9–1.2 nm). At large s, where the molecule is rather stretched in the junction with the most elongated (all-*trans*) configuration dominating, there is no marked temperature dependence. However, at intermediate s values, where the molecule can explore a whole range of different conformers, a notable temperature dependence is observed. In this s range, a number of conformers of B can bridge the gap and the temperature dependence then arises from a combination of the temperature-dependent conformer distribution and different conductance values for differing conformers, as described in detail in refs 14,15. At small s, the molecule becomes quite restricted in the junction and the temperature dependence is again suppressed. It should also be noted that the conductance of B is much smaller than that of A over the whole s range, in spite of the much smaller electrode separation. This, of course, is due to the pronounced difference in electronic structure between the two molecules.

The foregoing results show that both temperature and contact separation can influence the conductance across single molecular junctions. The molecular wire A has a rigid molecular backbone and the measured conductance shows no marked temperature dependence from room temperature to 77 °C. In contrast, the flexible molecule B shows pronounced temperature dependence, provided the contact separations allow the molecule to explore a range of different conformations, each presenting a differing conductance. As switching between conformers is rapid, the temperature dependence of I_M arises from the distribution of conformers, which is shifted towards the higher-energy (more eclipsed) conformers as the temperature is

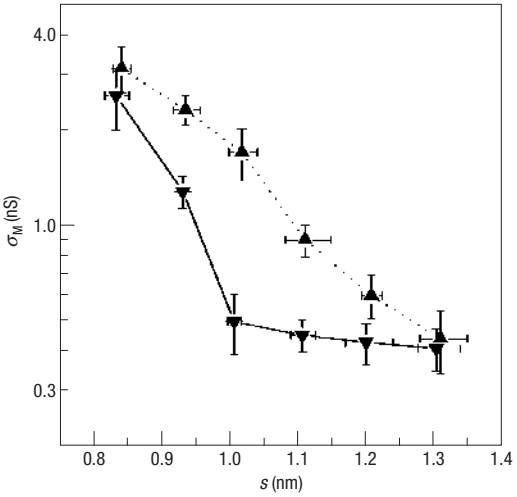

Figure 3 Single-molecule conductance. Nonanedithiol measured at 75 °C (up triangles) and 28 °C (down triangles) in dependence on s at $U_{tip} = +0.6$ V. Error bars represent the standard deviation of group 1 events.

increased. This mechanism for temperature dependence of the molecular conductance has recently been discussed[14,15]. The data presented here demonstrate that this temperature dependence can be suppressed by squeezing the molecule or by fully extending the molecule in the junction. Both have the consequence of reducing the conformational mobility of the molecular wire. These observations, and especially the finding that σ_M of a conformationally rigid molecule does not show any temperature dependence, corroborate the interpretation of temperature-dependent single-molecule conductance resulting from temperature-induced changes of the conformational distribution[14].

The $\sigma_M(\theta)$ data for molecule A (Fig. 2c) show that there is no measurable increase in the conductance as the molecule is tilted from 20 to 35°, followed by a conductance increase of an order of magnitude as the molecule is further tilted from 35 to 55°. The effect of tilt angle on molecular conductance has previously been theoretically considered for benzene-1,4-dithiolate (BDT) and –S–CH_2–C_6H_4–CH_2–S– (XDT) between gold contacts. For BDT, Kornilovitch and Bratkovsky[16] predict a large conductance increase on tilting the molecule from 0 to 90° (Figure 2 in ref. 16). Geng *et al.*[17] noticed no conductance increase for the case of BDT on tilting from 0 to 20°, followed by a small increase on further tilting to 30°. These theoretical observations for BDT are in qualitative agreement with the results presented here for molecule A.

To further understand the measured θ-dependence for molecule A, we have carried out a detailed theoretical investigation of electron transport through molecule A attached between a pair of (111) gold electrodes, using the recently developed, *ab initio*, non-equilibrium Green's function, SMEAGOL method[18,19]. Three possible sulphur sites above the (111) gold surfaces are considered, namely a top site, located directly above a gold atom, a hollow site, located above the centre of a triangle of gold atoms, and a bridge site, located between two neighbouring gold atoms. The energetically most favourable of these is the hollow site and therefore we begin by examining the case of hollow sites at both the gold substrate and gold tip. Figure 4a shows the transmission coefficient $T(E)$ for electrons of energy E passing through such a structure, for values of the tilt angle θ ranging from 10 to 70°. As θ increases, the highest occupied molecular orbital and

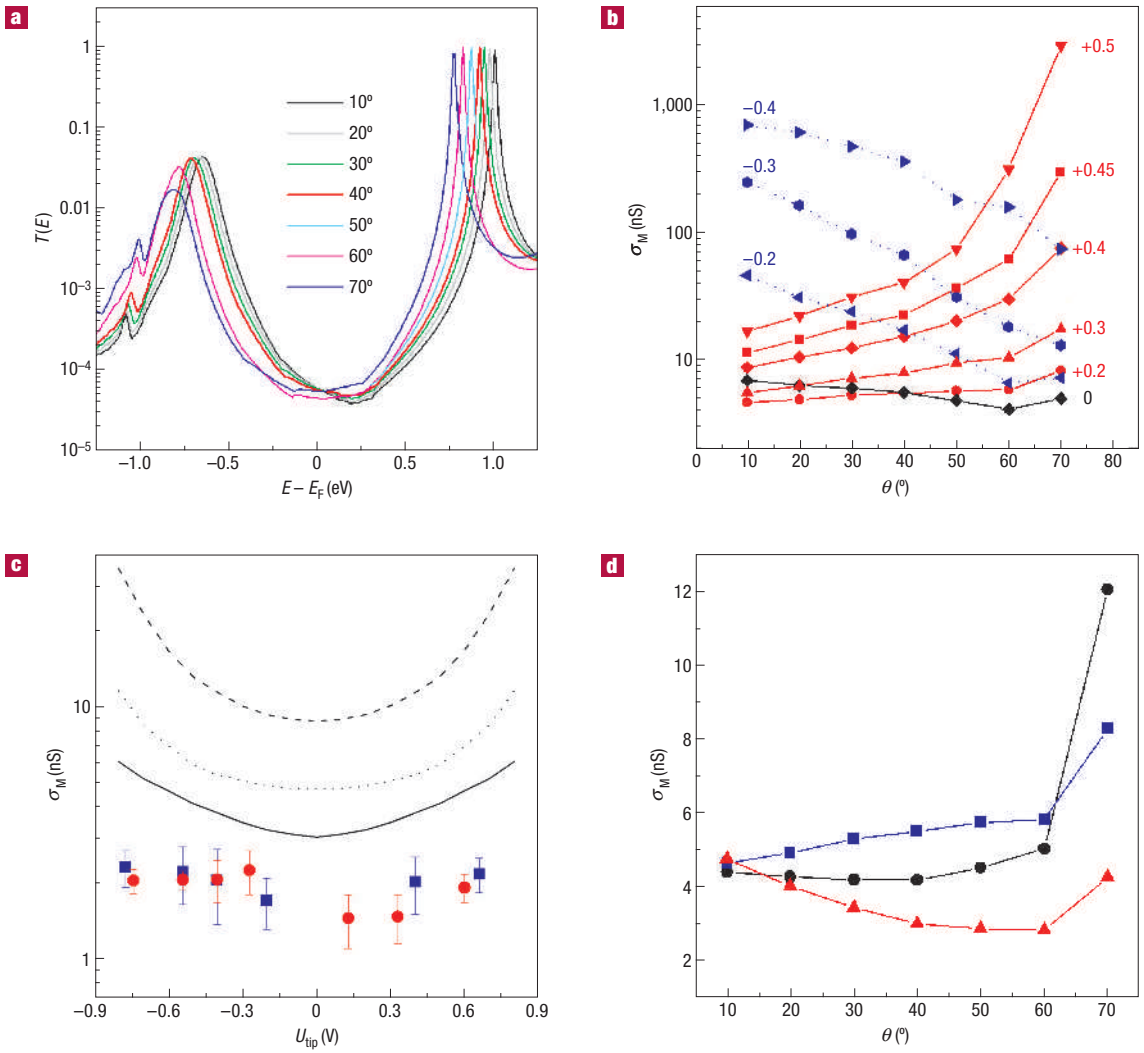

Figure 4 Calculated electron-transport characteristics for molecule A contacted between two parallel Au(111) electrodes in three-fold hollow sites. a, Transmission coefficient versus energy for tilt angles θ ranging from 10 to 70°. **b**, Single-molecule conductance of A at $U_{tip} = +0.6$ V obtained by averaging $T(E)$ from $E = E_F - 0.3$ V to $E = E_F + 0.3$ V for different positions of the Fermi level. **c**, Voltage dependence of the single-molecule conductance obtained by averaging $T(E)$ from $E = E_F - U_{tip}/2$ to $E = E_F + U_{tip}/2$ for different positions of the Fermi level; solid line $E_F = +0.2$ V; dotted line $E_F = 0$ V; dashed line $E_F = +0.5$ V. The experimental data at 22 °C (blue squares) and 65 °C (red circles) are shown for comparison. Error bars represent the standard deviation of group 1 events. **d**, Conductance of A at $E_F = +0.2$ V versus tilt angle for three different contact positions: hollow to hollow (blue squares), hollow to top (black circles) and top to top (red triangles).

lowest unoccupied molecular orbital resonances broaden and shift to lower energies, indicating that the strength of the coupling between gold surfaces and the molecule increases with increasing θ. For values of energy between 0.1 and 0.6 eV, $T(E)$ increases with increasing angle, in agreement with experiment. In contrast, for values of E between approximately 0.1 and −0.7 eV, $T(E)$ decreases with increasing angle. For this reason, we have treated the Fermi level E_F as a free parameter.

Figure 4b shows our results for the θ-dependence of $\sigma_M = (2e^2/h)T(E_F)$, for different positions of the Fermi level E_F. The shape of the $\sigma_M(\theta)$ plots in Fig. 4b is in qualitative agreement with the experimental findings for a Fermi level shift towards positive energy relative to the computed Fermi energy $E_F^0 = 0$ (see 'Details of the DFT Calculations' in the Methods section). In contrast, a shift towards negative energy values results in $\sigma_M(\theta)$ plots that are contrary to the experiment. This shows that the tilt-angle dependence of the conductance can act as a probe of the Fermi-level position, relative to the highest occupied molecular orbital and lowest unoccupied molecular orbital peaks.

The calculated voltage dependence of σ_M at a tilt angle of 10° for different positions of the Fermi level is shown in Fig. 4c together with the experimental data derived from Fig. 2d. The best fit of $\sigma_M(V)$ is achieved at a Fermi-level position of +0.2 V. Also, the form of the experimental $I_M(V)$ curve is reproduced best at this position of the Fermi level, as can be seen from the line in Fig. 2d. A shift of E_F to larger positive values would not just result in too large conductance values at low tilt angles but also in a much too steep dependence of σ_M on V as compared with the experimental data. This suggests that SIESTA slightly underestimates E_F, presumably because the underlying density functional theory (DFT) implementation does not contain self-interaction corrections, which in turn results in the notorious tendency of the DFT formalism to underestimate the highest occupied molecular orbital–lowest unoccupied molecular orbital

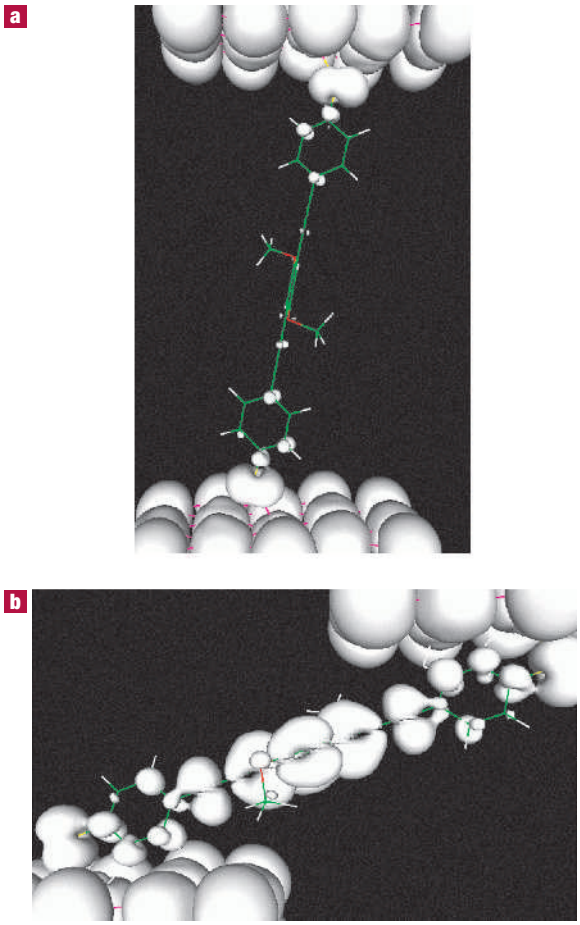

Figure 5 Surfaces of constant density of states for molecule A adsorbed to Au(111) for two different tilt angles. a, $\theta = 10°$; **b**, $\theta = 70°$. Three-fold hollow adsorption sites, $E = +0.2$ V and $U_{tip} = 0.6$ V in **a** and **b**.

gap, resulting in too large $T(E)$ values. This may explain why the theoretical results had to be divided by a factor of 2.3 to fit the experimental data in Fig. 2d.

With these findings in mind, we calculated $\sigma_M(\theta)$ at a Fermi-level position of +0.2 V for three different adsorption sites, as shown in Fig. 4d. For the case of threefold hollow adsorption sites, the conductance increases by a factor of two on a change in tilt angle from 10 to 70°. This increase in conductance is accompanied by a pronounced increase of the density of states at E_F, as is evident in Fig. 5, which depicts the surfaces of constant density of states at E_F for a tunnelling voltage of 0.6 V for $\theta = 10°$ (Fig. 5a) and $\theta = 70°$ (Fig. 5b).

Although these calculations provide a good fit for the $\sigma_M(\theta)$ plot from Fig. 2a for tilt angles up to ~35°, the experimentally observed steep increase for large tilt angles is not found in these calculations. To understand why the measured θ-dependence is much steeper than the theoretical result beyond $\theta \sim 35°$, we have examined the dependence of σ_M on the angle (α) between the planes of the central phenyl ring and the outer (coplanar) phenyl rings of the molecule. This angle is approximately 60° for the free molecule (geometry B in Fig. 6a). On a change from this geometry to a geometry where all three rings are coplanar (geometry A in Fig. 6a), the conductivity was found to increase by approximately an order of magnitude.

All of the above results correspond to the case where the plane containing the end phenyl rings is perpendicular to the (111) plane for all θ. We have also examined the effect of rigidly rotating the whole molecule about its axis by an angle ϕ. For an angle of $\phi = 0°$ the plane of the end phenyl rings lies perpendicular to the gold (111) surface and for $\phi = 90°$ the end phenyl rings lie almost parallel to the gold surface. As shown in Fig. 6b, the conductance increases significantly with increasing ϕ. In principle, the calculated dependence of σ_M on α could be a result of either changes in the hybridization between the terminal sulphur atoms and the gold contact, resulting in stronger electronic coupling from the contact into the molecular wire, or a change of the tunnelling path. Figure 6c,d shows the density of states at the Fermi energy for $\phi = 30°$ and 70° and demonstrates that the main source of the ϕ-dependence is an increased hybridization of the thiol and phenyl end groups with gold surface states.

In the preceding theoretical analysis, we have treated the adsorption geometry of the molecule A as static, but the energy barriers for rotations about ϕ and α are expected to be in the order of kT at 300 K. For example, the energy barrier for rotation of the neighbouring phenyl rings in a free tolane molecule was calculated to be only 37 meV and tolanethiols between metal contacts show rotations on the picosecond scale at 30 K according to molecular dynamic calculations[20]. Taking into account the fast fluctuations of ϕ and α, the experimentally measured conductance may be compared with the probability weighted values of $\sigma_M(\theta)$ with respect to ϕ and α. However, the dependence of σ_M on both ϕ and α helps to explain the experimental results. As θ increases beyond ~35°, geometrical constraints on the end groups and the central phenyl ring will cause ϕ to increase and α to decrease. Both of these effects will result in a steepening of the calculated dependence of σ_M on θ, in agreement with the experimental observations.

It is shown here that mapping of single-molecule conductance in dependence on molecular conformation in conjunction with the corresponding calculations can act as a spectroscopic probe to determine the position of the Fermi level with respect to the molecular orbital energies, and it has been demonstrated that the dependence of σ_M on temperature and contact separation can be minimized through a combination of molecular orientation and engineered molecular rigidity. Nevertheless, it should be kept in mind that contact fluctuations have to be reduced for single-molecule electrical junctions to facilitate their use as active components in room-temperature electronic devices.

METHODS

DETAILS OF THE DFT CALCULATIONS

Starting from the X-ray crystal structure of molecule A, we found the relaxed geometry of the molecule using the density functional code SIESTA. We used a single-zeta basis, Troullier–Martins pseudopotentials and the Ceperley–Alder local-density-approximation description of the exchange–correlation, and relaxed the atomic positions until all force components were smaller than 0.02 eV Å^{-1}. We then extended the molecule, by including five layers of the gold leads. We chose each layer, comprising 15 atoms, to provide a large enough surface area to include the effects of creating a large tilt angle. The extended regions of five layers of gold are sufficient to allow a suitable representation of the charge transfer effects at a molecule–gold interface. Using the recently developed, '*ab initio*', non-equilibrium Green's function, SMEAGOL method[18,19], we then computed electron transport coefficients. Initially, we chose a value of 2.1 Å as the gold–sulphur bond length; this is the optimum length for a hollow site (sulphur atoms sitting in the middle of three gold atoms). We investigated transport for three different contact geometries: hollow to hollow, where the bottom and top contacts are both located in a hollow site, hollow to top and top to top. In all three configurations we keep the contact distance the same. We then computed the conductance for tilt angles up to 70° with respect to the gold surfaces for the three different contact locations. We

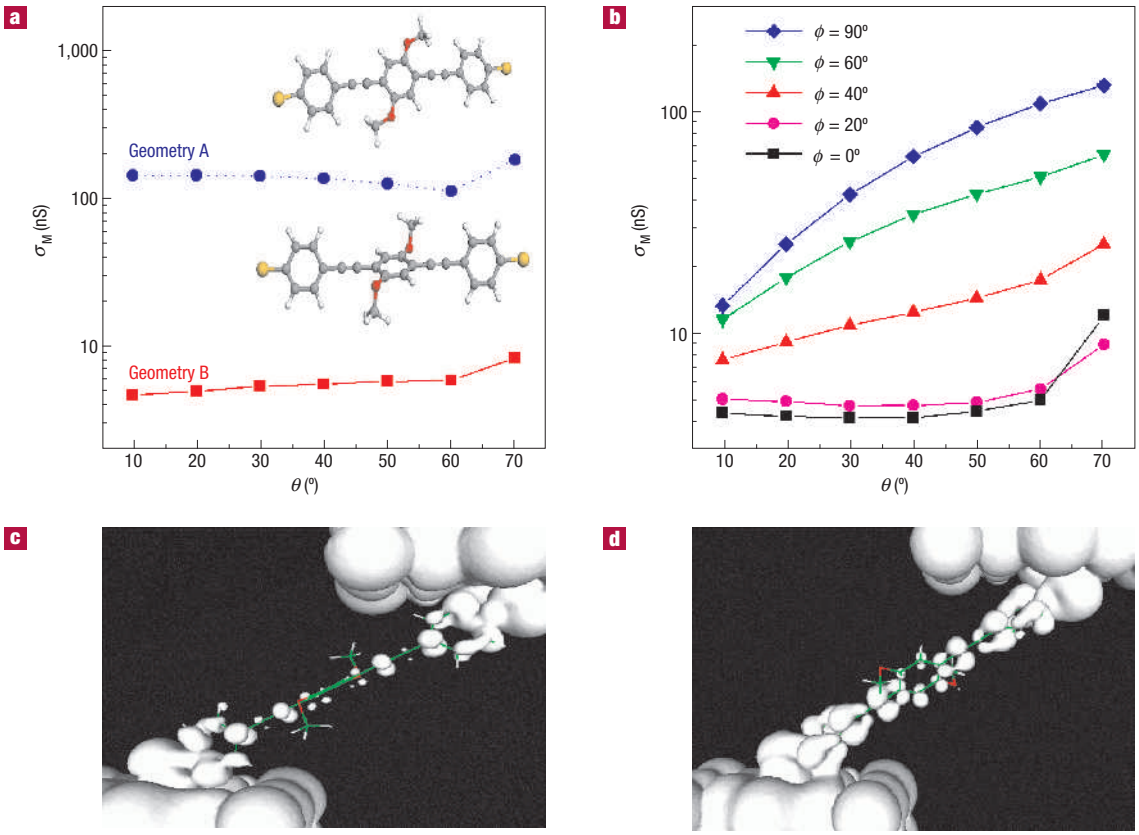

Figure 6 Electrical conductance of molecule A calculated in dependence on the contact geometry. a, Conductance versus θ for two orientations of the central phenyl ring. Geometry A (blue circles) corresponds to the three rings being almost coplanar and geometry B (red squares) corresponds to an angle $\alpha = 59^\circ$ between the central and outer rings. **b**, Conductance versus θ for five rigid rotations ϕ of the molecule about its axis bonded on hollow-to-top sites. For an angle of $\phi = 0^\circ$ (black squares) the plane of the end phenyl rings lies perpendicular to the gold (111) surface and for $\phi = 90^\circ$ (blue diamond) the end phenyl rings lie almost parallel to the gold surface. **c**,**d**, Density of states at the Fermi energy for $\phi = 30^\circ$ (**c**) and $\phi = 70^\circ$ (**d**). **c** and **d** demonstrate that the main source of the ϕ-dependence is an increased hybridization of the thiol and phenyl end groups with gold surface states.

kept the direction of the tilt across the gold surface the same in all calculations to reduce the possible number of configurations. Using SIESTA, we computed the local density of states at the Fermi energy for different values of θ and ϕ.

DETAILS OF THE $s(I_0)$ CALIBRATION

To provide a reliable calibration of the relative tip–sample distance (s–s_0) versus I_0, we recorded several $I(s)$ scans during each experiment (that is with the molecules adsorbed on the sample). For calibration purposes, we selected 20 of these $I(s)$ scans in which no signs of wire formation could be found (see Fig. 1f as an example), as I_0 is by definition the current flowing between tip and sample in the absence of a molecular wire (compare Fig. 1a and b). We used linear regression to determine the slope of $\ln(I_0)$ versus s in the I_0 range that was relevant to the experiment. We then averaged the 20 slope values to yield a value of $-(5.4 \pm 1.5)$ nm^{-1} for A and $-(8.1 \pm 1.9)$ nm^{-1} for B. We calibrated the z piezo elongation factor by measuring the height of monoatomic steps on Au(111) (0.236 nm per step was assumed). For calibration of the absolute separation between the Au electrodes we determined the critical current (I_c), that is to say the I_0 value for which the molecule cannot bridge the gap. We assumed that at I_c the molecule is oriented perpendicular on the Au(111) surface and adsorbed at both ends in threefold hollow sites with an Au–S distance of 0.21 nm consistent with theory. We determined the S–S distance (2.01 nm for A and 1.30 nm for all-*trans* nonanedithiol) with a molecular modelling program (SPARTAN).

SYNTHETIC PROCEDURES AND SAMPLE PREPARATION

We synthesized the wire molecule A in Durham using a novel protocol and characterized its structure by elemental analysis, NMR spectroscopy and single-crystal X-ray diffraction as detailed in the Supplementary Information. We immersed gold samples in a 5×10^{-5} M solution of A in THF for 10 s, washed them with ethanol and blew them dry in a stream of nitrogen. Before the immersion, we flame annealed the gold-on-glass samples at ~1,000 °C for 60 s, a procedure that is known to result in atomically flat ⟨111⟩-oriented terraces[21].

Received 9 May 2006; accepted 5 October 2006; published 26 November 2006.

References

1. Cui, X. D. *et al.* Reproducible measurement of single-molecule conductivity. *Science* **294,** 571–574 (2001).
2. Haiss, W. *et al.* Measurement of single molecule conductivity using the spontaneous formation of molecular wires. *Phys. Chem. Chem. Phys.* **6,** 4330–4337 (2004).
3. Haiss, W. *et al.* Redox state dependence of single molecule conductivity. *J. Am. Chem. Soc.* **125,** 15294–15295 (2003).
4. Xu, B. Q. & Tao, N. J. J. Measurement of single-molecule resistance by repeated formation of molecular junctions. *Science* **301,** 1221–1223 (2003).
5. Weber, H. B. *et al.* Conductance properties of single-molecule junctions. *Physica E* **18,** 231–232 (2003).
6. Reichert, J. *et al.* Driving current through single organic molecules. *Phys. Rev. Lett.* **88,** 176804 (2002).
7. Metzger, R. M. *et al.* Unimolecular electrical rectification in hexadecylquinolinium tricyanoquinodimethanide. *J. Am. Chem. Soc.* **119,** 10455–10466 (1997).
8. Feldheim, D. L. & Keating, C. D. Self-assembly of single electron transistors and related devices. *Chem. Soc. Rev.* **27,** 1–12 (1998).
9. Klein, D. L., Roth, R., Lim, A. K. L., Alivisatos, A. P. & McEuen, P. L. A Single-electron transistor made from a cadmium selenide nanocrystal. *Nature* **389,** 699–701 (1997).
10. Chen, J., Reed, M. A., Rawlett, A. M. & Tour, J. M. Large on-off ratios and negative differential resistance in a molecular electronic device. *Science* **286,** 1550–1552 (1999).
11. Collier, C. P. *et al.* Electronically configurable molecular-based logic gates. *Science* **285,** 391–394 (1999).
12. Andres, R. P. *et al.* "Coulomb" staircase at room temperature in a self-assembled molecular nanostructure. *Science* **272,** 1323–1325 (1996).

13. Haiss, W. *et al.* Molecular wire formation from viologen assemblies. *Langmuir* **20,** 7694–7702 (2004).
14. Haiss, W. *et al.* Thermal gating of the single molecule conductance of alkanedithiols. *Faraday Discus.* **131,** 253–264 (2006).
15. Kornyshev, A. A. & Kuznetsov, A. M. Single molecule tunnelling conductance: the temperature and length dependences controlled by conformational fluctuations. *Chem. Phys.* **324,** 276–279 (2006).
16. Kornilovitch, P. E. & Bratkovsky, A. M. Orientational dependence of current through molecular films. *Phys. Rev. B* **64,** 195413 (2001).
17. Geng, W. T., Nara, J. & Ohno, T. Impacts of metal electrode and molecule orientation on the conductance of a single molecule. *Appl. Phys. Lett.* **85,** 5992–5994 (2004).
18. Rocha, A. R. *et al.* Spin and molecular electronics in atomically-generated orbital landscapes. *Phys. Rev. B* **73,** 085414 (2006).
19. Reily Rocha, A. *et al.* Towards molecular spintronics. *Nature Mater.* **4,** 335–339 (2005).
20. Seminario, J. M., Zacarias, A. G. & Tour, J. M. Theoretical interpretation of conductivity measurements of a thiotolane sandwich. A molecular scale electronic controller. *J. Am. Chem. Soc.* **120,** 3970–3974 (1998).
21. Haiss, W., Lackey, D., Sass, J. K. & Besocke, K. H. Atomic resolution scanning tunneling microscopy images of Au(111) surfaces in air and polar organic-solvents. *J. Chem. Phys.* **95,** 2193–2196 (1991).

Acknowledgements

This work was supported by EPSRC (Mechanisms of Single Molecule Conductance) (Liverpool), Basic Technology (Controlled Electron Transport) (Durham and Lancaster) and a Lancaster–EPSRC Portfolio Partnership and MCRTN Fundamentals of Nanoelectronics.
Correspondence and requests for materials should be addressed to W.H.
Supplementary Information accompanies this paper on www.nature.com/naturematerials.

Competing financial interests

The authors declare that they have no competing financial interests.